UCRL-53419
Distribution Category UC-11,92,92a

Mechanical Properties of Mesaverde Sandstone and Shale at High Pressures

W. Lin

Manuscript date: April 1, 1983

LAWRENCE LIVERMORE NATIONAL LABORATORY
University of California · Livermore, California · 94550

Available from: National Technical Information Service • U.S. Department of Commerce
5285 Port Royal Road • Springfield, VA 22161 • $8.50 per copy • (Microfiche $4.50)

CONTENTS

Mechanical Properties of Mesaverde Sandstone and Shale at High Pressures

ABSTRACT

This report covers the mechanical properties of Mesaverde rock (shale and sandstone) core samples from various depths in five wells in Colorado and Wyoming. The properties studied were tensile strength, compressive strength, hydrostatic compressibility, shear stress under one-dimensional strain compression, and static elastic moduli. With respect to these properties, the sandstones are virtually isotropic. The shales, on the other hand, are definitely anisotropic. The nature and degree of anisotropy of the shales vary with the depth of sample origin. In addition, the relative values of these mechanical properties between the shale and the sandstone also vary with depth.

1. INTRODUCTION

It is estimated that low-permeability western gas reservoir and eastern Devonian shales in the U.S. contain large quantities of natural gas. In order to recover these resources economically, the region around a production well must be stimulated to induce a more rapid flow of the natural gas into the well bore. Currently, the most promising techniques for stimulating low-permeability gas reservoirs is with fluids under pressure[1].

The goal of the Unconventional Gas Program at the Lawrence Livermore National Laboratory (LLNL) is to obtain a more detailed understanding of the stimulation processes. Current methods for predicting intensity, geometry, and extent of fracturing resulting from hydraulic stimulation require certain equation-of-state (EOS) measurements as input data to the calculation codes. The purpose of this report is to present the laboratory determined EOS data on Mesaverde sandstone and shale core samples obtained at various depths from vertical boreholes drilled in Colorado and Wyoming.

The mechanical properties studied in this report were tensile strength at 0.1 MPa, compressive strength as a function of confining pressure up to 400 MPa, stress-strain behavior under one-dimensional (1-D) strain compressive loading, and pressure-volume behavior under hydrostatic compression up to a confining pressure of 1.2 GPa.

2. ROCK DESCRIPTION AND SAMPLE PREPARATION

2.1 ROCK DESCRIPTION

Table 1 lists the well locations and the depth at which the core samples were obtained. The rocks are grouped according to well locations. The rock types along with their group numbers will be used throughout this report for ease of identification.

The cores contain alternating sections of sandstone and shale. Generally, bedding planes in the pure sandstone and shale sections are not clear. We assume that the bedding plane is parallel to the interface between the sandstone and shale sections and is usually horizontal. Table 2 summarizes the grain size, color, and dry-bulk and grain density of the rock types. The sandstone sections of the cores are usually quite homogeneous. On the other hand, some of the shale sections, for instance, Shale I and Shale II, show variations of color and dry-bulk and grain density. No grain size data is available for the shale samples.

The mineral composition of the rocks listed in Table 3 was by determined by x-ray analysis. This table also shows that the quartz content of the sandstone increases and varies with depth. Shales IV and V contain almost as much quartz as the corresponding sandstones. At a depth less than 1958 m, the shale usually contains larger amounts of clay minerals, such as illite, kaolinite, montmorillonite, etc., than the sandstone. The rocks from deeper than 1958 m contain no more than a trace amount of clay minerals.

2.2 SAMPLE PREPARATION

All of our test specimens were right cylinders. The lenght and diameter of the specimens, as shown in Table 4, was dependent on the type of test and the availability of initial core material.

The specimens were recored from initial samples and then cut into sections. The ends were ground parallel to within 0.02 mm. The specimens were then dried in a vacuum oven at a temperature of about 30°C until their weights remained unchanged for at least one day. The dry bulk densities, as listed in Table 2, were calculated from the dry weight and specimen dimensions.

Table 1. Location and depth of Mesaverde formation rock samples used in this study.

Rock	Group	Well name	Location	Depth (m)
Sandstone	I	Twin Arrow C&K 4-14	Rio Blanco, CO	352
Shale	Ia	"	"	350
	Ib	"	"	368
Sandstone	II	PTS 24-19 Federal	Sublette, WY	1582
Shale	IIa	"	"	1580
	IIb	"	"	1599
Sandstone	III	PTS 22-12 Federal	Rio Blanco, CO	1958
Shale	III	"	"	1968
Sandstone	IV	PTS 3-10-1	Sweetwater, WY	3512
Shale	IV	"	"	3511
Sandstone	V	Rainbow Resources 1-3 Federal	Sweetwater, WY	3795 3805
Shale	V	"	"	3883

Table 2. Grain sizes, colors, and densities of the Mesaverde rocks.

Rock	Grain size	Color	Dry-bulk density (Mg/m^3)	Grain density (Mg/m^3)
Sandstone I	∿ 0.5mm	beige	2.094 ± 0.011	2.676
Shale Ia	Very fine	black grey-grey	2.254 ± 0.056	2.3450
Shale Ib	Very fine	grey	2.457 ± 0.068	2.684
Sandstone II	∿ 0.1-0.2mm	grey	2.546 ± 0.006	2.73
Shale IIa	Very fine	grey to dark grey	2.575 ± 0.021	2.66
Shale IIb	Very fine	dark grey	2.505 ± 0.012	2.64
Sandstone III	∿ 0.2-0.2mm	light grey	2.345 ± 0.011	2.69
Shale III	Very fine	grey	2.660 ± 0.007	2.69
Sandstone IV	∿ 0.1mm	light grey	2.536 ± 0.004	2.71
Shale IV	Very fine	dark grey	2.610 ± 0.012	2.89
Sandstone V	0.2-0.3mm	light grey	2.407 ± 0.016	2.87
Shale V	Very fine	grey to dark grey	2.516 ± 0.016	2.92

Table 3. Mineral composition of mesaverde rocks determined by x-ray analyses.

Rock	Mineral composition
Sandstone I	Quartz (75%), illite-muscovite (15%), kaolinite-nacrite (10%), bytownite or anorthite (10%), montmorillonite (trace)
Shale Ia	Quartz (75%), illite-muscovite (15%), kaolinite-nacrite (5%), bytownite or anorthite (5%)
Shale Ib	Quartz (35%), rhodochrosite-siderite (35%) illite-muscovite (15%), bytownite or anorthite (10%), colomite-amberite (5%)
Sandstone II	Quartz (80%), kaolinite-nacrite (13%), illite-muscovite (5%), montmorillonite (trace)
Shale II	Quartz (65%), illite-muscovite (15%) kaolinite-nacrite (10%), dolomite (5%), calcite (1-5%), montmorillonite (trace)
Sandstone III	Quartz (95%), calcite (Trace), plagioclase-oligoclase (trace), kaolinite (trace)
Shale III	Quartz (85%), calcite (10%), paglioclase-oligoclase (trace), kaolinite (trace)
Sandstone IV	Quartz ($\sim$ 100%), plagioclase - oligoclase (trace)
Shale IV	Quartz (95%), plagioclase - oligoclase (trace), kaolinite (trace)
Sandstone V	Quartz ($\sim$ 100%)
Shale V	Quartz ($\sim$ 100%), calcite (trace), kaolinite (trace)

Table 4. Specimen dimensions (diameter x length), in mm, of Mesaverde rocks used in various types of tests.

Rock	Brazilian test	Compressive strength	Pressure-volume	1-D strain
Sandstone I	12.7 x 6.4	19.05 x 40.0	12.7 x 28.0	
shale I	12.7 x 6.4	19.05 x 40.0	12.7 x 28.0	
Sandstone II	19.1 x 9.5	19.05 x 40.0	19.05 x 25.4	19.05 x 40.0
Shale II	19.1 x 9.5	19.05 x 40.0	19.05 x 25.4	19.05 x 40.0
Sandstone III	19.1 x 9.5	19.05 x 40.0	19.05 x 25.4	19.05 x 40.0
Shale II	19.1 x 9.5	19.05 x 40.0	19.05 x 25.4	19.05 x 40.0
Sandstone IV	19.1 x 9.5	19.05 x 40.0	19.05 x 25.4	19.05 x 40.0
		12.7 x 40.0		
Shale IV	19.1 x 9.5	19.05 x 40.0	19.05 x 25.4	19.05 x 40.0
Sandstone V	19.1 x 10.0	12.5 x 35.0	19.07 x 26.0	19.07 x 38.8
Shale V	19.1 x 10.0	12.5 x 35.0	19.04 x 26.5	19.05 x 38.9

For determination of compressive strength under triaxial compressive loading, the specimens were jacketed in 0.32-cm-thick Tygon tubing.

To determine the stress-strain relations under 1-D strain loading and the pressure-volume behavior under hydrostatic compression, the specimens were encapsulated in annealed copper jackets approximately 0.12-mm thick. To eliminate the gap between the jacket and the specimen, the jacketed specimens were then seasoned to a pressure of about 0.7 MPa for several hours After seasoning, two pairs of electrical-resistance strain gages were mounted on the jacket near the middle of the specimens to measure longitudinal and radial strains. For the measurement of stress-strain relations under 1-D strain loading, on specimens cored parallel to bedding, a pair of radial strain gages were oriented so that they measured strain in the direction of bedding.

3. EXPERIMENTAL PROCEDURES

For the determination of tensile strength using the Brazilian test, the disc-type specimens were loaded diametrically until failure. Thin cardboard, approximately 0.5-mm thick, was put between the specimen and hardened-steel loading platens to distribute the load over an arc of about 15 degrees. This decreased the stress concentration at the point of loading so that the likelihood of failure by shear at the contacts were decreased. The distributed load had virtually no effect on the stresses in the specimen[2]. We loaded the specimen slowly (about 0.02 to 0.05 MPa/s) and released the load when the specimen showed sign of failure. We were able to generate a diametrical crack in the middle of each specimen thus satisfying the criterion of the Brazilian test.[3] Total load and diametrical (parallel to loading) displacement were recorded on an x-y recorder. Tensile strength (σ_t) was calculated from the total load (F) by

$$\sigma_t = \frac{F}{\pi r l}$$

where r and l are radius and length of a specimen, respectively. The tensile strength was determined both parallel and perpendicular to bedding.

To determine the compressive strength of a specimen, as a function of confining pressure, we axially loaded the Tygon-jacketed specimen until failure, keeping the confining pressure constant. The differential load (axial load minus confining pressure) and axial displacement were recorded on an x-y recorder. An internal load cell was used to measure the axial load. The axial displacement was measured by an external linear-displacement gage. Differential stress was determined by dividing the differential load by the cross-sectional area of a specimen. Shear stress is one half of this value. When a specimen exhibited brittle failure the compressive strength of specimen was calculated at the point of the maximum differential load on the load vs. displacement curve. When a specimen exhibited ductile deformation and work hardening was present, we arbitrarily chose the differential stress at a shortening of 5% beyond the linear, elastic deformation as the compressive strength of the specimen. To correct the change of the cross sectional area of a specimen due to the axial compressive loading, we assumed that all strains are homogeneous and the volume of the specimen remained

constant before failure. Therefore, the change of the cross-sectional area was linearly proportional to the axial displacement. The compressive strength of the Tygon jacket was insignificantly small at pressures below 0.3 GPa (less than 1.6 MPa for a specimen 19.1-mm in diameter). However, the strength of the jacket increased to an equivalent of about 8.0 MPa (on a 19.1-mm sample) and 20 MPa (on a 19.1-mm sample) at confining pressures of 0.35 GPa and 0.4 GPa respectively. The compressive strength was corrected for all specimens at pressures greater than 0.35 GPa.

Because of their sedimentary nature, the Mesaverde rocks were assumed to be transversely isotropic at the onset of testing, with one principal axis of stress and strain being perpendicular to bedding and the other two parallel to the bedding. Then the five stiffnesses of the material can be determined from 1-D strain-compression tests. The linear elastic stress and strain components are related by the following equation with z-direction perpendicular to the bedding and the x- and t-directions parallel to bedding:

$$
\begin{aligned}
\sigma_x &= C_{11}\,\varepsilon_x + (C_{11} - 2\,C_{66})\,\varepsilon_y + C_{13}\,\varepsilon_z \\
\sigma_y &= (C_{11} - 2\,C_{66})\,\varepsilon_x + C_{11}\,\varepsilon_y + C_{13}\,\varepsilon_z \\
\sigma_z &= C_{13}\,\varepsilon_x + C_{13}\,\varepsilon_y + C_{33}\,\varepsilon_z \\
\tau_{yz} &= C_{44}\,\gamma_{yz} \\
\tau_{zx} &= C_{44}\,\gamma_{zx} \\
\tau_{xy} &= C_{66}\,\gamma_{xy} \quad ,
\end{aligned}
\tag{1}
$$

where σ_x, σ_y, and σ_z are normal stresses; τ_{yz}, τ_{zx}, and τ_{xy} are shear stresses; ε_x, ε_y, and ε_z are normal strains, γ_{yz}, γ_{zx}, and γ_{xy} are shear strains; C_{ij} are stiffnesses[2]. For a cylindrical specimen cored perpendicular to the bedding under a 1-D strain loading i.e. $\varepsilon_x = \varepsilon_y = o$, $\sigma_y = \sigma_x =$ confining pressure (P), σ_z = longitudinal stress (σ_ℓ), and ε_z = longitudinal strain (ε_ℓ), (1) becomes

$$
\begin{aligned}
P &= C_{13}\,\varepsilon_\ell \\
\sigma_\ell &= C_{33}\,\varepsilon_\ell \\
1/2\,(\sigma_\ell - P) &= C_{44}\,\varepsilon_\ell
\end{aligned}
\tag{2}
$$

From Eq. (2), C_{13}, C_{33}, and C_{44} can be determined. For a cylindrical specimen cored parallel to bedding, with radial strain gage mounted parallel to bedding, under 1-D strain loading (say in the y-direction), $\varepsilon_x = o$, $\sigma_x = \sigma_z = P$, $\sigma_y = \sigma_\ell$, $\varepsilon_y = \varepsilon_\ell$, then (1) becomes

$$
\begin{aligned}
\sigma_\ell &= C_{11}\,\varepsilon_\ell + C_{13}\,\varepsilon_z \\
P &= C_{13}\,\varepsilon_\ell + C_{33}\,\varepsilon_z \\
1/2\,(\sigma_\ell - P) &= C_{66}\,\varepsilon_\ell
\end{aligned}
\tag{3}
$$

The experimental procedures of 1-D strain measurement were as follows. The copper-jacketed specimens, with mounted strain gages, were loaded hydrostatically to an initial confining pressure of 20 to 50 MPa. The axial load and confining pressure were then simultaneously manually increased such that the absolute radial strain of a specimen remained within $\pm$ 10 x 10^{-6}. In most cases, the radial strain was kept within $\pm$ 5 x 10^{-6}. We usually loaded the specimens to a maximum pressure of about 0.3 GPa. During a test, σ_ℓ, P, ε_ℓ and radial strain (ε_r) were recorded by a microcomputer when ε_r was zero.

The σ_ℓ, P, and $\tau = 1/2\,(\sigma_\ell - P)$ determined in an 1-D strain experiment loaded perpendicular to bedding were fitted with a third order polynomial equations in terms of ε_ℓ.

The slope of the fitted curves,

$$
\frac{d\sigma_\ell}{d\varepsilon_\ell}, \quad \frac{dp}{d\varepsilon_\ell}, \text{ and } \quad \frac{d\tau}{d\varepsilon_\ell}
$$

were C_{33}, C_{13}, and C_{44} respectively. The elastic stiffnesses C_{33}, C_{13}, and C_{44} were then plotted as functions of confining pressure. Similarly, σ_ℓ, P, and τ of a specimen loaded parallel to bedding were

fitted with a polynomial in terms of ε_ℓ. The slope,

$$\frac{d\tau}{d\varepsilon_\ell}$$

yielded C_{66}. The slopes

$$\frac{d\sigma_\ell}{d\varepsilon_\ell} \text{ and } \frac{dP}{d\varepsilon_\ell}$$

along with C_{33} and C_{13} determined in the test loaded perpendicular to bedding were used to calculate C_{11}:

$$C_{11} = \frac{d\sigma_\ell}{d\varepsilon_\ell} \frac{C_{13}}{C_{33}}\left(\frac{dp}{d\varepsilon_\ell} - C_{13}\right) \tag{4}$$

The values of C_{33} and C_{13} in Eq. (4) were interpolated from the C_{33} vs P and C_{13} vs. P curves at pressures corresponding to the values of ε_ℓ determined in the experiment where loading was parallel to bedding.

For engineering applications, elastic moduli are more commonly used. The elastic moduli matrix, [Sij], is the inverse of the stiffness matrix,

$$[Sij] = [Cij]^{-1}.$$

Therefore

$$\begin{aligned} S_{11} &= (C_{11} C_{33} - C_{13}^{\,2})/D \\ S_{12} &= [C_{13}^{\,2} - (C_{11} - 2 C_{66}) C_{33}]/D \\ S_{13} &= -2 C_{13} C_{66}/D \\ S_{33} &= 4 C_{66} (C_{11} - C_{66})/D \\ S_{44} &= 1/C_{44} \\ S_{66} &= 1/C_{66}, \end{aligned} \tag{5}$$

where

$$D = \begin{vmatrix} C_{11} & (C_{11} - 2 C_{66}) & C_{13} \\ (C_{11} - 2 C_{66}) & C_{11} & C_{13} \\ C_{13} & C_{13} & C_{33} \end{vmatrix} = 4 C_{66}[C_{33}(C_{11} - C_{66}) - C_{13}^{\,2}].$$

The Young's moduli (E_x, E_y, and E_z), shear moduli (G_{xy}, G_{xz},

and G_{yz}) and Poisson's ratios (ν_{xy}, ν_{xz}, and ν_{zx}) of the material can be obtained as

$$\begin{aligned} E_x &= E_y = 1/S_{11} \\ E_z &= 1/S_{33} \\ G_{xz} &= G_{yz} = 1/S_{44} \\ \nu_{xy} &= -S_{12}/S_{11} \\ \nu_{xz} &= -S_{13}/S_{11} \end{aligned} \tag{6}$$

From these parameters in Eq. (6) we can calculate $G_{xy} = E_x/2(1+\nu_{xy})$ and $\nu_{zx} = E_z \cdot \nu_{xz}/E_x$.

The short, strain-gaged specimens (Table 4) were used to determine the P-V behavior under hydrostatic compression. Longitudinal strain (ε_ℓ) and radial strain (ε_r) were measured as a function of confining pressure up to 1.2 GPa. A LSI-11 microcomputer was used for the data acquisition. The volumetric strain (ε_v) was calculated as $\varepsilon_v = \varepsilon_\ell + 2\,\varepsilon_r$. For an isotropic or transversely isotropic rock the volumetric strain so measured on a cylindrical specimen cored perpendicular to bedding is the true volumetric strain under hydrostatic compression.

4. RESULTS AND DISCUSSION

4.1 TENSILE STRENGTH

Tensile strengths of Mesaverde rocks at 0.1 MPa, which do not seem to have a clear relation with the depth of the sample origin, are summarized in Table 5. The tensile strengths for the Mesaverde rocks from a depth shallower than 1958 m, the sandstone has smaller tensile strength than the shale. On the other hand, for the rocks from a greater depth, the sandstone is stronger than the shale. Generally speaking, the sandstone exhibits little anisotropy in tensile strength. The shale, however, loaded parallel to bedding is stronger than that loaded perpendicular to bedding. The tensile strength of most of the rocks (Table 5) have small values of one standard deviation, indicating that the rocks are homogeneous and Brazilian testing gives consistent results. The great value of one standard deviation of the tensile strength of shale I is due to rock inhomogeneity.

With reference to Table 5, the tensile strengths of sandtones are within the range as compiled by Rummel[4]. The tensile strength of sandstone IV is greater than that of Wagon Wheel No. 1 sandstone from a depth of 3120 m[5]. The tensile strength of Sandstone III is almost twice of that of the sandstones from Project Rio Blanco (from a depth range of 1782 m to 1942 m)[6].

4.2 COMPRESSIVE STRENGTH

Compressive strength was determined from the axial load-displacement curves. Typical behavior of the Mesaverde rocks under triaxial compressive loading are illustrated by Fig. 1. Brittle behavior, illustrated by Fig. 1(a), may be characterized by a sudden change of slope of the load-displacement curve at the yield point, followed by a sharp downward break in the curve. Ductile behavior, illustrated by Fig. 1(b), is taken to be the absence of any sharp downward breaks in slope after the yield point, with the

Table 5. Tensile strength of Mesaverde rocks at atmospheric pressure.

Rock	Depth (m)	Number of tests	Parallel (//) perpendicular (⊥)	Averaged tensile strength (MPa), and standard deviation
Sandstone I	353	13	//	3.29 ± 0.56
		20	⊥	3.19 ± 0.45
Shale I	350	12	//	11.51 ± 3.21
	354	7	⊥	8.83 ± 4.53
Sandstone II	1582	12	//	8.71 ± 0.75
		11	⊥	8.62 ± 1.25
Shale II	1576	9	//	16.52 ± 2.64
		12	⊥	10.73 ± 2.37
Sandstone III	1958	9	//	6.92 ± 0.41
		6	⊥	6.06 ± 0.22
Shale III	1958	9	//	18.6 ± 1.3
		12	⊥	17.3 ± 3.6
Sandstone IV	3510	10	//	19.2 ± 1.7
		10	⊥	16.4 ± 1.7
Shale IV	3510	10	//	18.6 ± 2.2
		10	⊥	9.6 ± 1.1
Sandstone V	3800	9	//	13.55 ± 0.74
		10	⊥	10.01 ± 0.75
Shale V	3880	5	//	8.51 ± 0.87
		7	⊥	5.42 ± 0.59

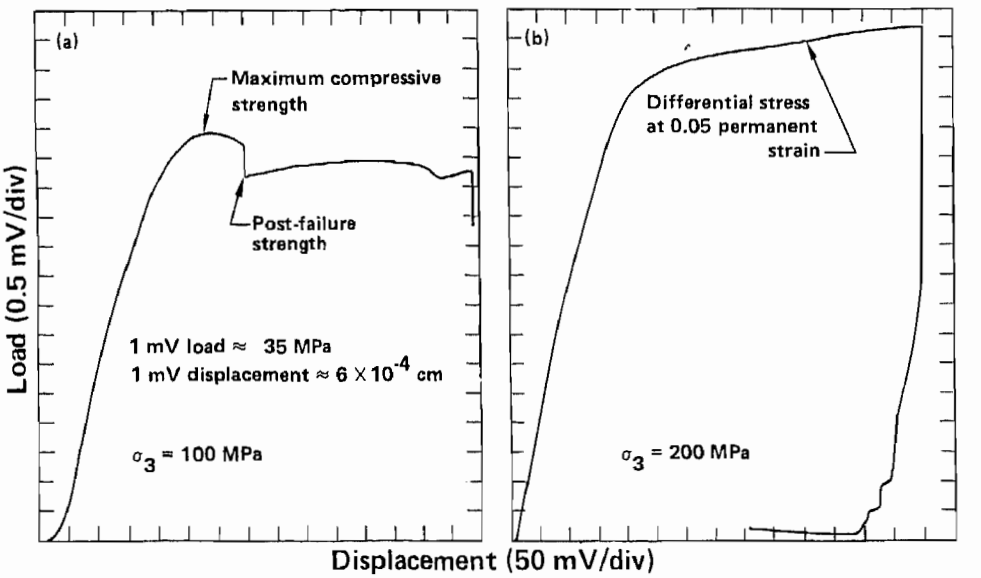

Fig. 1. The failure mode of a smaple under compressive strength test may be brittle at low pressure (a) and ductile at high pressure (b).

specimen achieving at least 5% permanent strain (beyond the linear elastic strain) before fracture. The compressive strength reported here is either the ultimate strength (in these tests exhibited brittle behavior) or the differential stress taken at 5% permanent strain (for those tests that were macroscopically ductile).

The compressive strength of Mesaverde rocks are shown in terms of shear stress, $(\sigma_1 - \sigma_3)/2$ where σ_1 and σ_3 are maximum principal stress and confining pressure respectively, in Figs. 2 through 11 of the Appendix. Each figure shows the compressive strength of a rock loaded both perpendicular and parallel to bedding. The rate of increase of compressive strength decreases with increasing confining pressure.

Generally speaking, Mesaverde sandstone shows little anisotropy in the compressive strength with respect to bedding. The greatest anisotropy in compressive strength of the sandstone is shown in Fig. 8, related to Sandstone IV. Even in this case, the compressive strengths loaded perpendicular and parallel to bedding do not differ by more than 10%. The Mesaverde shale shows some anisotropy in compressive strength. The degree of anisotropy appears to vary with the depth of sample origin. Shale I when loaded perpendicular to bedding is about 30% stronger than loaded parallel to bedding. Shale II has no significant anisotropy in compressive strength. But Shale IIa is about 40% stronger than shale IIb. Shale III when loaded parallel to bedding is about 10 to 20% stronger than loaded perpendicular to bedding. The two deeper shale samples are also somewhat anisotropic, but with less degree (about 10%).

The relative compressive strength between sandstone and shale varies with depth. For the rocks from a depth of 350 m (Figs. 2 and 3) the sandstone has a compressive strength about 30% smaller than the shale when loaded perpendicular to bedding. When loaded parallel to bedding both rocks have about the same strength. For the rocks from a depth of 1580-m to 1599-m (Figs.4 and 5), Shale IIa from a depth of 1580 m is about 20% stronger than the sandstone from a depth of 1582 m (Sandstone II), which in turn, is about 10% stronger than the Shale IIb from a depth of 1599 m. Rocks from the depth range of 1958- to 1968-m (Figs. 6 and 7), the shale loaded perpendicular to bedding has about the same strength as the sandstone; the shale loaded

parallel to bedding is about 30% stronger than the sandstone. From the depth of 3510 m (Figs. 8 and 9), however, the sandstone is about twice as strong as the shale. The sandstone from a depth of 3800 m is about 40 to 60% stronger than shale from a depth of 3880 m (Figs. 10 and 11).

The confining pressure at which the transition between brittle failure and ductile deformation occurs depends on rock type, the depth of origin, and (to some extent) direction of loading. Table 6 lists the pressure at which the brittle-ductile transitions occur. These pressures are all greater than the overburden pressure of these rocks.

To compare with some previously studied Mesaverde sandstones, the strength of the dry Equity So. Sulfur Creek sandstone (from a depth of 1942 m)[6] is about 50 to 70% weaker than sandstone III (from a depth of 1958 m). Sandstone IV (from a depth of 3510-m) is about 30 to 50% stronger than the Wagon Wheel No. 1 sandstone (from a depth of 3120 m)[5].

4.3 PRESSURE-VOLUME BEHBAVIOR

The typical volumetric strain vs pressure behavior of the Mesaverde rocks under hydrostatic compression is shown in Figs. 12 through 14 of the Appendix. The volumetric strain of the unloading path is greater than for the loading path. This indicates inelastic compaction of the rock. The difference in volumetric strain between loading and unloading paths depends on rock type and maximum pressure. When a specimen is unloaded to 0.1 MPa there is always some residual strain. It also depends on rock type and maximum pressure. The volumetric strain of the sandstone in the loading path clearly shows a discontinuity of compressibility at pressure below 0.1 GPa. The volumetric strain data of the shale show continuous decrease in compressibility. This may due to different microscopic structure between the sandstone and the shale. Table 7 summarizes the maximum volumetric strain, residual strain, and bulk modulus at the overburden pressure for these rocks.

Figure 12 represents the typical pressure-volume (P-V) behavior of Sandstones I and III. The non-linear P-V behavior is similar to that of a porous material. At pressures below 0.3 GPa the compressibility of the sandstone decreases with increasing pressure. This may be due to the closing

Table 6. Brittle-ductile transition confining pressure under triaxial compression.

Rock Type	Transition pressure (MPa)	
	Parallel to bedding	Perpendicular to bedding
Sandstone I	80-100	100-125
Sandstone II	210-240	260-300
Sandstone III	100-125	130-150
Sandstone IV	(>300)	(>300)
Sandstone IV	380-400	300
Shale I	250-270	250-270
Shale IIa	-	200-220
Shale IIb	140-160	150-200
Shale III	300-350	300-350
Shale IV	(>400)	400
Shale V	300-350	250-300

Table 7. Maximum volumetric strain (ε_M), residual volumetric strain (ε_R), and bulk modulus (K_B) at overburden pressure of Mesaverde rocks under hydrostatic compression.

Rock type	Maximum pressure (GPa)	ε_M (%)	ε_R (%)	Overburden pressure (MPa)	K_B (GPa)
Sandstone I	1.2	11.8	2.3	8.0	2.8
Shale I	1.2	7.3	1.3	8.0	8.4
Sandstone II	0.7	5.2	1.9	40.0	8.5
Shale IIa	0.7	4.4	1.3	40.0	13.4
Shale IIb	0.7	5.2	1.7	40.0	7.9
Sandstone III	0.7	5.1	0.5	50.0	9.0
Shale III	0.7	2.8	0.6	50.0	18.2
Sandstone IV	0.76	3.4	0.3	90.0	23.8
Shale IV	0.75	2.7	0.3	90.0	19.1
Sandstone V	0.8	4.2	0.7	98.0	19.4
Shale V	0.8	5.1	1.2	98.0	10.5

up of grain boundary microcracks. At pressure between 0.3 GPa and 0.7 GPa the compressibility of the sandstone increases with increasing pressure. This is an indication of pore collapse. At pressures greater than 0.7 GPa the compressibility of the sandstone decreases with increasing pressure, indicating that the specimen has become a solid with fewer pores and narrow cracks. Even though Sandstone I and Sandstone III have similar volumetric strain vs pressure curve, Sandstone I is more compressible than Sandstone III (Table 7). This is consistent with the total porosities of these two rocks (Table 2). The typical P-V behavior of the other sandstones (II, IV, and V) is shown in Fig. 13. The volumetric strain data are similar to that of a low porosity solid. There is a clear discontinuity of compressibility at a pressure about 0.07 GPa. Otherwise, the compressibility decreases continuously with increasing pressure. The total porosity of Sandstone V is rather great, about 16% (Table 2). One possible explanation is that most of the porosity of Sandstone V might be due to large aspect ratio pores.

Figure 14 shows the typical P-V behavior of the shales. The data show a continuous decrease of compressibility with increasing pressure. As shown in Table 7, Shale IV is the least compressible one; Shale I and IIb are similar, being the most compressible ones.

4.4 ONE-DIMENSIONAL STRAIN COMPRESSION

Due to the shortage of cores we did not test Sandstone I and Shale I under 1-D strain loading conditions. The typical 1-D strain testing results, in terms of shear stress, $(\sigma_1 - \sigma_3)/2$, vs pressure (σ_3) plot are shown in Figs. 15 to 17 (Appendix). Each of these figures shows the result of one rock type when loaded both perpendicular and parallel to bedding. Comparison with the failure envelopes shown in Figs. 2 to 11, the shear stress under 1-D strain loading is always smaller than the maximum strength of the rocks. Figures 15 to 17 show that the shear stress increases rapidly with increasing confining pressure at the beginning of loading. At further loading, the slope of the shear stress gradually decreases. This may indicate the increase of inelasticity in the deformation under 1-D strain loading[6]. The sandstone also has a steeper slope of $(\sigma_1 - \sigma_3)/2$ vs σ_3 than the shale from same depth.

Figure 15 shows that the shear stress of Sandstone II, under 1-D strain loading, is independent of the loading direction. Other rocks investigated show that shear stress depends somewhat on direction of loading. Figure 16 shows the typical result of Sandstone III and IV and Shales II, III, and IV. Here, when loaded parallel to bedding, these specimens exhibit a greater shear stress than when loaded perpendicular to bedding. Figure 17 represents the results of Sandstone V and Shale V. In this case, the specimens loaded perpendicular to bedding show a greater shear stress than when loaded parallel to bedding.

Young's moduli (E_x and E_z), shear moduli (G_{xy} and G_{xz}), and Poisson's ratios (ν_{xy}, ν_{xz}, and ν_{zx}) were calculated as function of pressure. It should be pointed out that Equation (1), and the equations thereafter, are based on the assumption of linear elasticity. The stress-strain relation of these 1-D strain measurements and the shear stress shown in Figs. 15 to 17 indicate that the specimens deform non-elastically and non-linearly over most of the loading range. Therefore, the calculated elastic parameters vary with pressure.

Table 8 summarizes the static elastic parameters of Mesaverde rocks at the beginning of loading and the overburden pressure. E_x and E_z of Mesaverde sandstone show little difference. This is consistent with the isotropic nature of the rock in other properties. The Young's moduli of the sandstone decrease with increasing pressure. On the other hand, for the shales E_x is greater than E_z except for shale IV. Similar to the sandstone, the Young's moduli of the shales also decrease with increasing pressure. The sandstones are stiffer than the shales in most cases. Shale III seems to be stiffer than sandstone III. In all of the rocks investigated, G_{xy} and G_{xz}, the shear moduli, decrease with increasing pressure. Schock et.al., reported similar findings in their studies of rocks from Wagon Wheel No. 1. and Rio Blanco Gas Stimulation Experiments[5,6]. The shear moduli of the sandstone show little anisotropy, consistent with other properties. The shear moduli of the shales show various degrees of anisotropy. For most of the shales, except Shale IV, G_{xy} is greater than G_{xz}. For Shale IV, G_{xz} is greater than G_{xy}. Sandstone III has shear moduli smaller than shale III. All of the other sandstones have shear moduli greater than that of the corresponding shales.

Table 8. Young's moduli (E_x, E_z), shear moduli (G_{xy}, G_{xz}), ad Poisson's ratios (ν_{xy}, ν_{xz}, and ν_{zx}) of Mesaverde rocks at the beginning of loading (P_1) and overburden pressure (P_o); all moduli and pressure are in GPa. As shown in the text, G_{xy} and ν_{zx} are not independent.

Rock	P_1/P_o	E_x	E_z	G_{xy}	G_{xz}	ν_{xy}	ν_{xz}	ν_{zx}
Sandstone II	$0.027/_{0.04}$	10.54	10.72	3.82	3.68	0.38	0.27	0.28
		10.45	10.3	3.80	3.66	0.37	0.30	0.29
Shale II	$0.015/_{0.04}$	8.54	7.47	3.34	2.75	0.28	0.35	0.31
		8.14	7.16	3.11	2.57	0.31	0.39	0.35
Sandstone III	$0.038/_{0.05}$	18.03	18.06	6.9	6.5	0.31	0.26	0.26
		17.07	16.91	6.57	6.11	0.31	0.27	0.27
Shale III	$0.105/_{0.05}$	31.65	20.09	12.95	6.2	0.22	0.46	0.29
		----	----	----	----	----	----	----
Sandstone IV	$0.018/_{0.09}$	45.14	45.22	19.45	19.1	0.16	0.16	0.16
		41.05	42.27	17.18	18.61	0.20	0.22	0.22
Shale IV	$0.017/_{0.09}$	23.78	26.68	8.86	12.4	0.34	0.049	0.055
		17.86	21.14	6.64	8.66	0.35	0.33	0.39
Sandstone V	$0.023/_{0.098}$	28.64	29.1	11.43	12.4	0.25	0.14	0.15
		23.36	21.82	9.23	7.67	0.27	0.25	0.23
Shale V	$0.017/_{0.098}$	11.17	8.31	4.61	2.85	0.21	0.43	0.32
		10.34	8.86	3.89	3.0	0.33	0.40	0.35

Poisson's ratios, of the rocks increase with increasing pressure. The only exception is ν_{xz} of Shale V which decreases from 0.43 to 0.4 when pressure increases from 17 MPa to 98 MPa. Schock also reported increase of Poisson's ratio with loading[6]. The differences between ν_{xz} and ν_{zx} of the sandstones are very small. This is another indication of the isotropic nature of the sandstones. For most of the shale specimens (Shale II, III, and V) ν_{xz} is greater than ν_{zx}. ν_{zx} of Shale IV is greater than ν_{xz}. The difference in Poisson's ratio of Shale IV from the other shales is consistent with the Young's moduli and shear moduli.

5. SUMMARY

The tensile strength of the Mesaverde rocks is not systematically dependent upon the depth of sample origin. But the relative tensile strength between the sandstone and shale depends on the depth of sample origin. For the rocks from depths shallower than 1985 m inclusive, the shale has a tensile strength greater than the sandstone, from about 20% to more than 300%. On the other hand, for the rocks from 3510-m and 3880-m depth the sandstone is stronger than the shale, from about 60 to 200%. The sandstones from depths shallower than 1985 m show little anisotropy in tensile strength. Within the same depth range, however, the shale loaded parallel to bedding is about 8 to 50% stronger than that loaded perpendicular to bedding. The sandstones from depths of 3510 and 3800 m, when loaded parallel to bedding, have tensile strength about 15 to 30% stronger than when loaded perpendicular to bedding. The shales from 3510- and 3880-m depths have tensile strength anisotropy ranges from 50 to 60%, parallel to bedding being the stronger direction.

The compressive strength of the sandstone is fairly isotropic. The only sandstone that shows some anisotropy in compressive strength is the one from 3510 m. In this case, the compressive strength loaded perpendicular to bedding is only about 10% greater than that loaded parallel to bedding. The compressive strength of the shales, however, shows various degrees of anisotropy with depth. Also, the anisotropy switches direction from loading perpendicular to bedding being stronger for the shale from 352-m depth to loading parallel to bedding being stronger for the shales from deeper than 1958 m. The relative compressive strength between the shale and the sandstone

also varies with the depth of sample origin. From depths shallower than 1958 m, the shale is stronger than the sandstone. The sandstone from depths greater than 3510 m is stronger than the shale.

The hydrostatic compressibilities of the shale and the sandstone show similar variations with depth as was noted for the compressive strength. The compressibility of the sandstone has a clear discontinuity at confining pressures below 0.1 GPa, whereas, the shales have a continuous decrease of compressibility with increasing pressure. The relative compressibility also changes from the sandstone being more compressible for the rocks from a depth shallower than 1958 m to the shale being more compressible for the rocks from greater depths.

1-D strain tests yield somewhat different results. The shear stress under 1-D strain loading is always smaller than the compressive strength of the rocks investigated. The shear moduli of these rocks decrease with increasing pressure. Poisson's ratios, on the other hand increase with increasing pressure. The sandstones are virtually isotropic in the elastic moduli and Poisson's ratios. But for the shales, again, strong anisotropy in these parameters is shown.

The anisotropic nature of the mechanical properties of the shales and the variation of the relative values of the properties between the shale and the sandstone with depth may have significant impact on the model analyses and prediction of the fracturing processes in the Mesaverde formation. One example is the effect of the sandstone-shale interface on fracture propagation. The direction of fracture propagation in the shale may be affected by their anisotropic properties.

6. ACKNOWLEDGMENTS

This research was performed as part of the Unconventional Gas Program of the Lawrence Livermore National Laboratory, Livermore, CA., The author is indebted to W. Beiriger for his determinations of the mineral composition, E. Britton for his measurements of the grain density of the rocks, and to F. Heuze's for his very helpful contribution to data analysis. The author is also grateful for the comments of H. Heard and M. Costantino.

This work was performed under the auspices of the U. S. Department of Energy by the Lawrence Livermore National Laboratory under contract W-7405-ENG-48.

7. REFERENCES

1. M. E. Hanson, , R. J. Shafer, G. D. Anderson, H. C. Heard, D. O. Emerson, C. Knutson, and B. Haimson, LLL Gas Stimulation Program Quarterly Progress Report, July through September 1977, Lawrence Livermore National Laboratory, Livermore, CA, UCRL-50036-77-3 (1977)

2. J. C. Jaeger and N. G. W. Cook, Fundamentals of Rock Mechanics," (Chapman and Hall, London, 1979), 3rd ed.

3. J. A. Hudson, E. T. Brown and F. Rummel, "The controlled failure of rock discs and rings loaded in diametral compression," Int. J. Rock Mech. Min. Sci. 9, 241-248 (1972).

4. F.Rummel, Fracture and flow of rocks and minerals, in physical properties of rocks, G. Angenheister, Ed., (Springer-Verlag, N.Y., 1982), subvolume b.

5. R. N. Schock, H. C. Heard, and D. R. Stephens, High-pressure mechanical properties of rocks from Wagon Wheel No. 1, Pinedale, Wy, Lawrence Livermore National Laboratory, Livermore, CA, UCRL-50963 (1970).

6. R. N. Schock, H. C. Heard, and D. R. Stephens, Mechanical Properties of rocks from the site of the Rio Blanco Gas Stimulation Experiment, Lawrence Livermore National Laboratory, Livermore, CA, UCRL-51260 (1972).

APPENDIX

FAILURE ENVELOPES OF MESAVERDE SANDSTONE AND SHALE

(Figures 2 to 11)

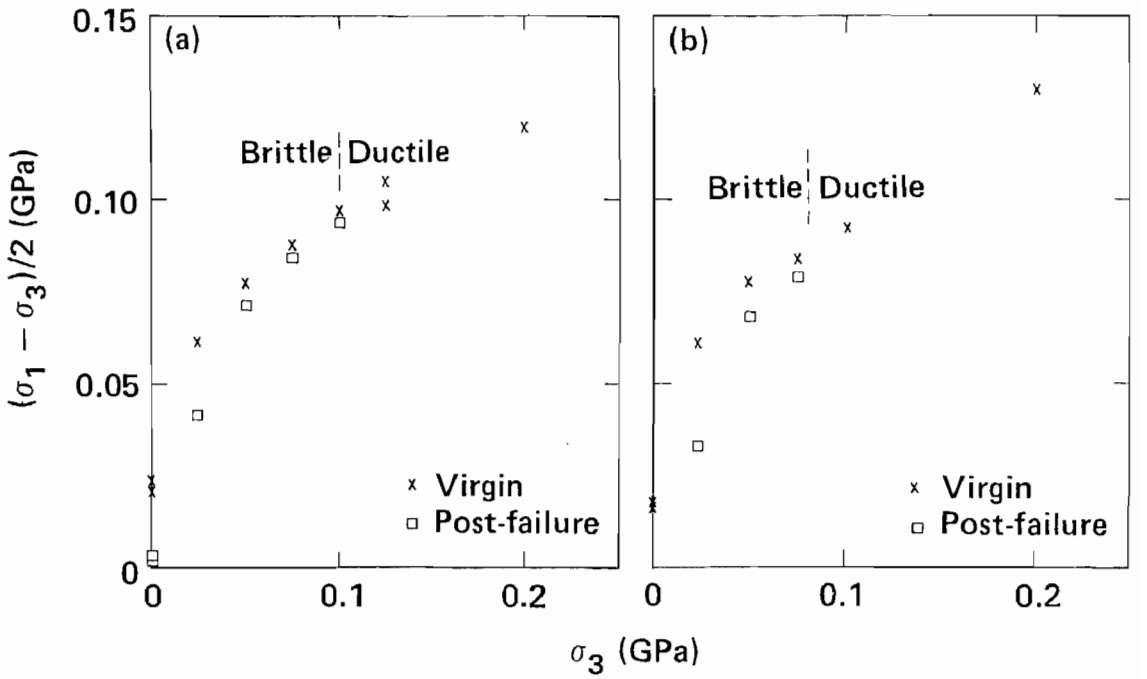

Fig. 2. Failure envelopes of Mesaverde Sandstone I, loaded perpendicular (a) and parallel (b) to bedding.

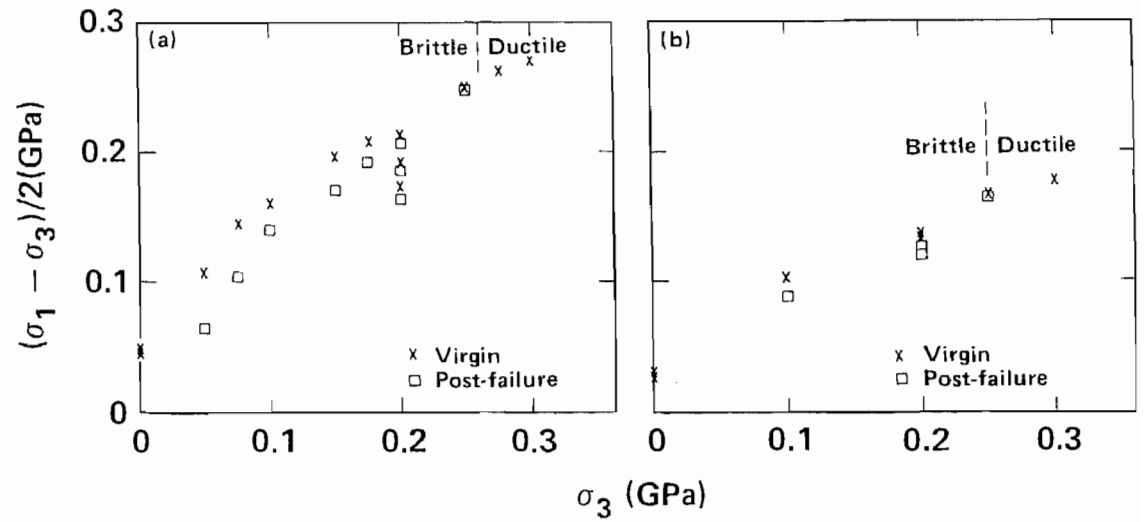

Fig. 3. Failure envelopes of Mesaverde Shale I, loaded perpendicular (a) and parallel (b) to bedding.

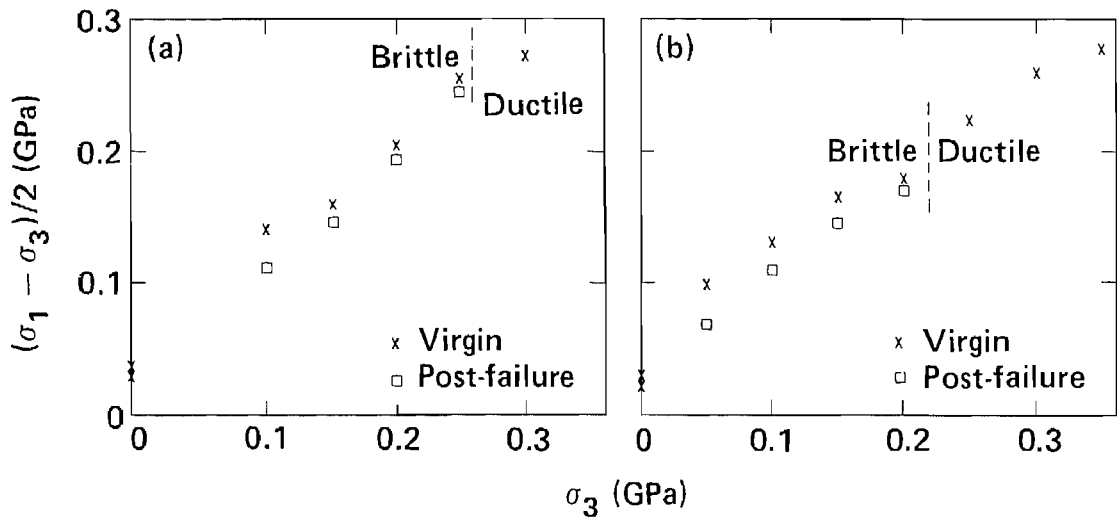

Fig. 4. Failure envelopes of Mesaverde Sandstone II, loaded perpendicular (a) and parallel (b) to bedding.

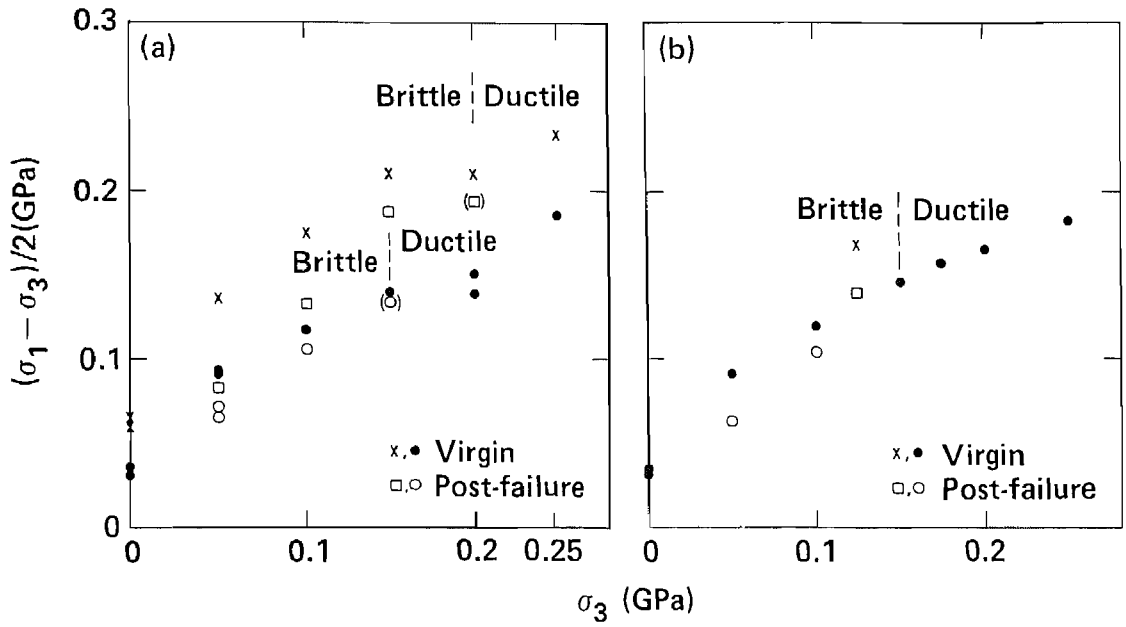

Fig. 5. Failure envelopes of Mesaverde Shale IIa (X and □) and IIb (• and o), loaded perpendicular (a) and parallel (b) to bedding.

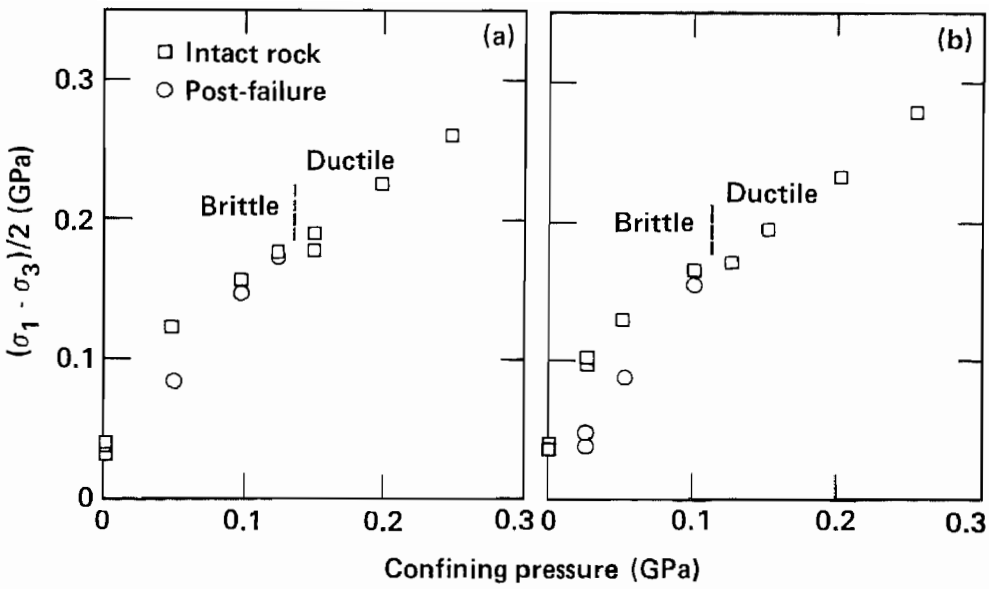

Fig. 6. Failure envelopes of Mesaverde Sandstone III, loaded perpendicular (a) and parallel (b) to bedding.

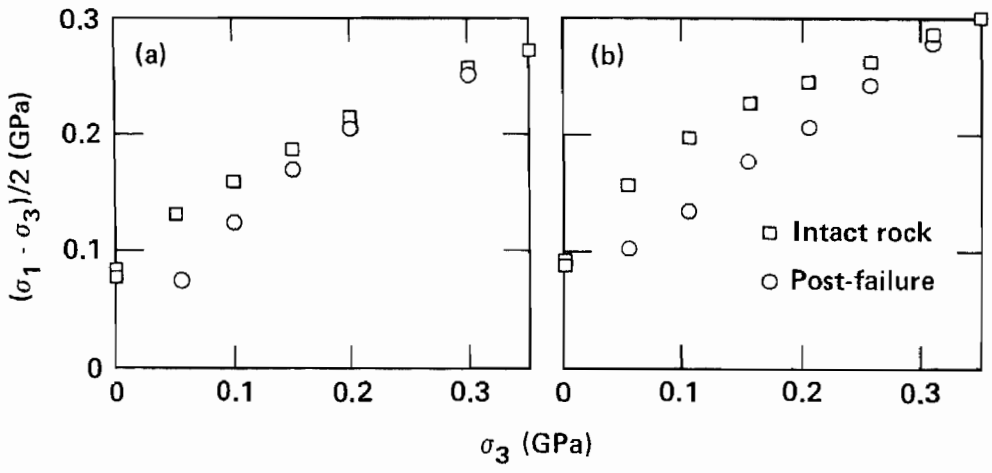

Fig. 7. Failure envelopes of Mesaverde Shale III, loaded perpendicular (a) and parallel (b) to bedding.

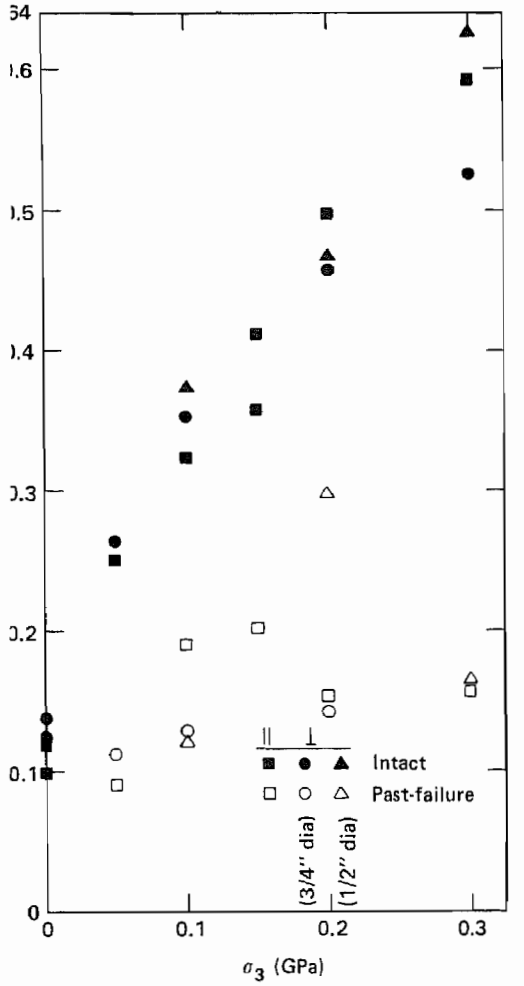

Fig. 8. Failure envelopes of Mesaverde Sandstone IV, loaded perpendicular (⊥) and parallel (∥) to bedding.

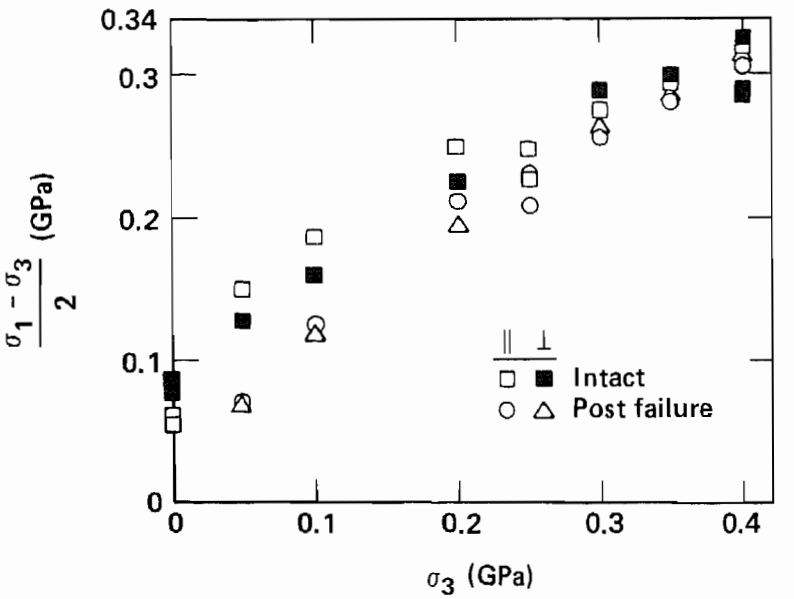

Fig. 9. Failure envelopes of Mesaverde Shale IV, loaded perpendicular (⊥) and parallel (∥) to bedding.

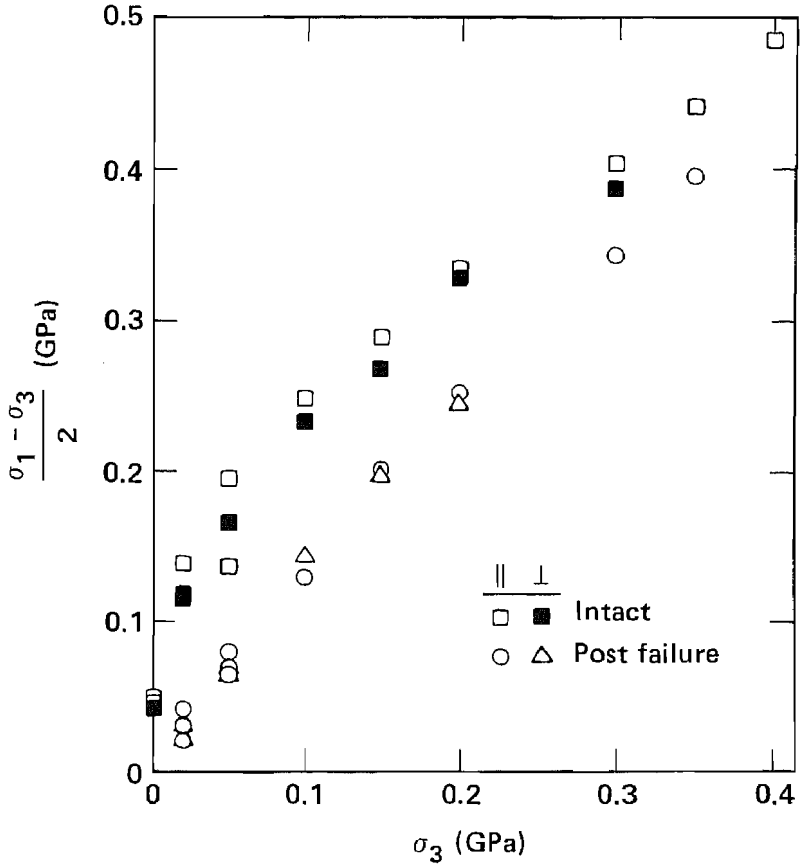

Fig. 10. Failure envelopes of Mesaverde Sandstone V, loaded perpendicular (⊥) and parallel (∥) to bedding.

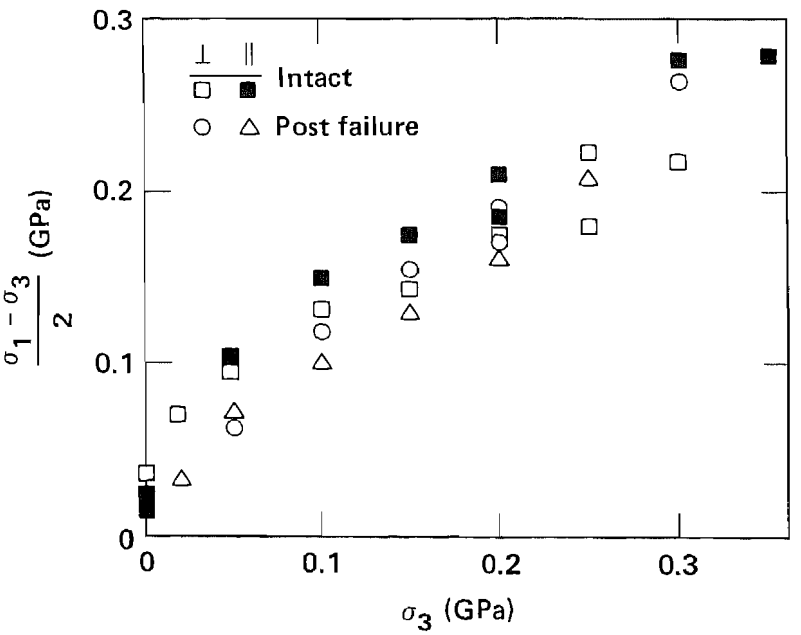

Fig. 11. Failure envelopes of Mesaverde Shale V, loaded perpendicular (⊥) and parallel (∥) to bedding.

APPENDIX

TYPICAL PRESSURE-VOLUME BEHAVIOR OF THE MEASAVERDE ROCKS UNDER HYDROSTATIC COMPRESSION

(Figures 12 to 14)

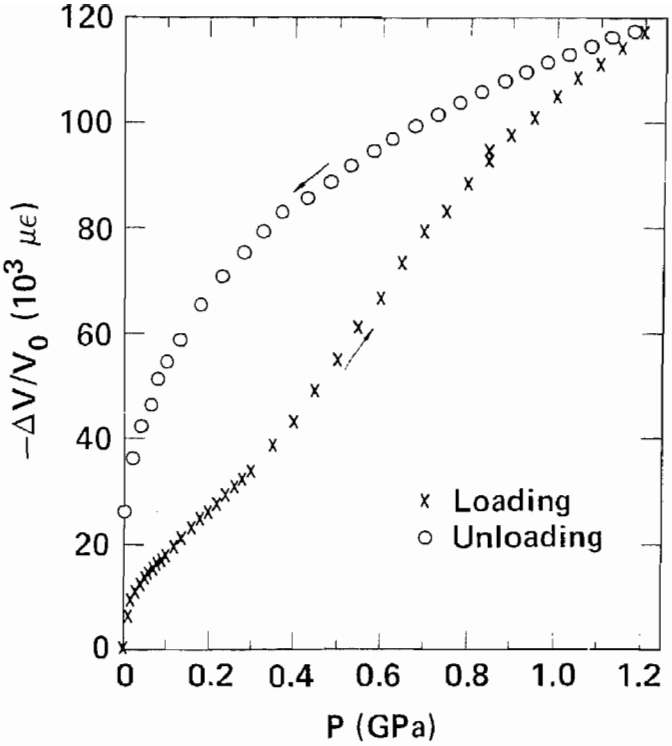

Fig. 12. Pressure-volume behavior of Sandstone I under hydrostatic compression represents the nonlinear characteristic.

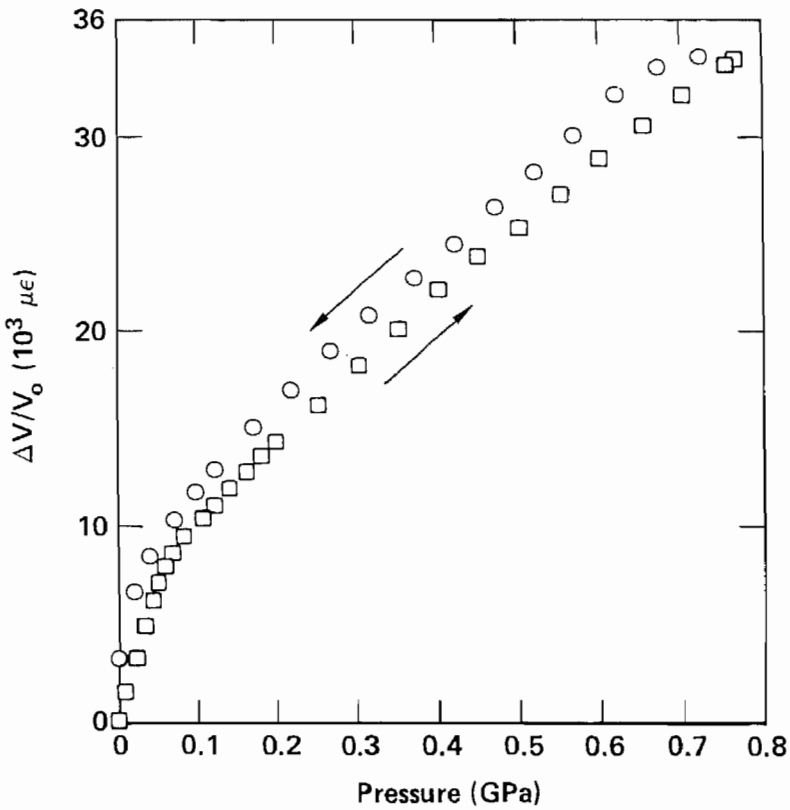

Fig. 13. Pressure-volume behavior of Sandstone IV under hydrostatic compression shows a discontinuity of compressibility at a pressure of less than 0.1 GPa.

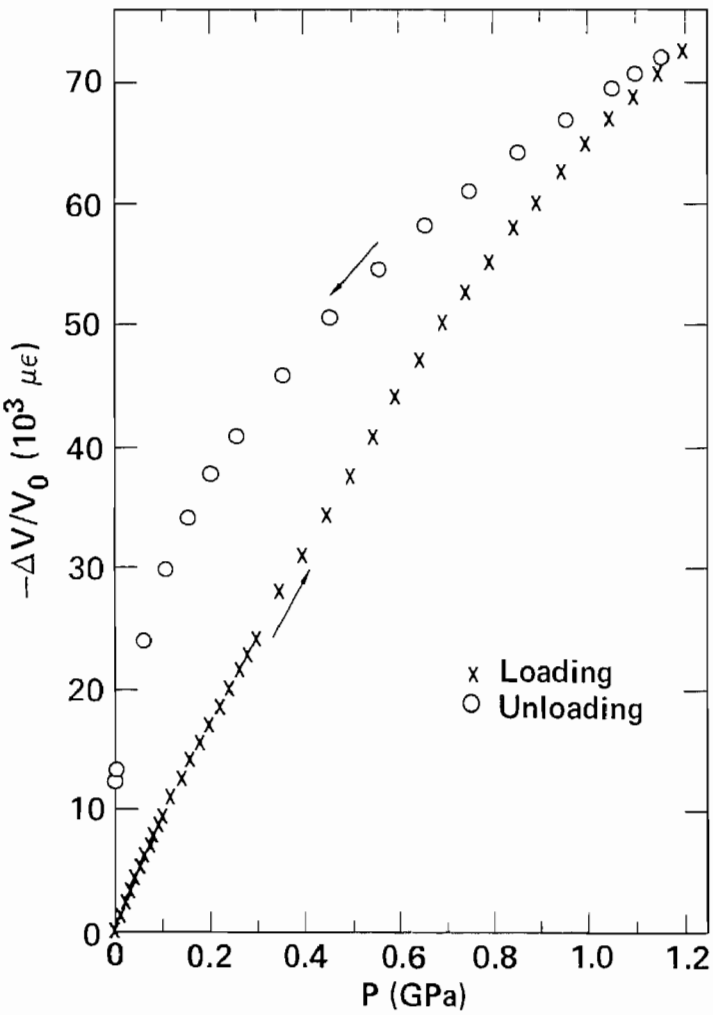

Fig. 14. Pressure-volume behavior of Shale I under hydrostatic compression shows continuous decrease of compressibility with increasing pressure.

APPENDIX

TYPICAL SHEAR STRESS VS PRESSURE PLOTS OF THE MESAVERDE ROCKS UNDER 1-D STRAIN COMPRESSION

(Figures 15 to 17)

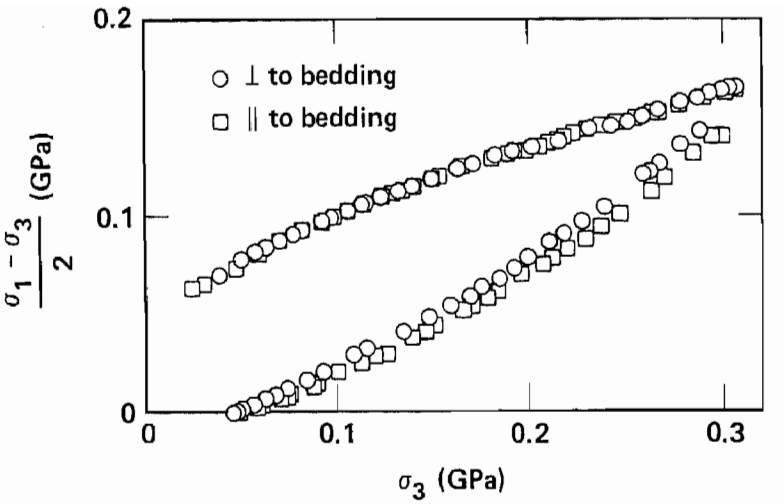

Fig. 15. Shear stress of Sandstone II under 1-D strain compression.

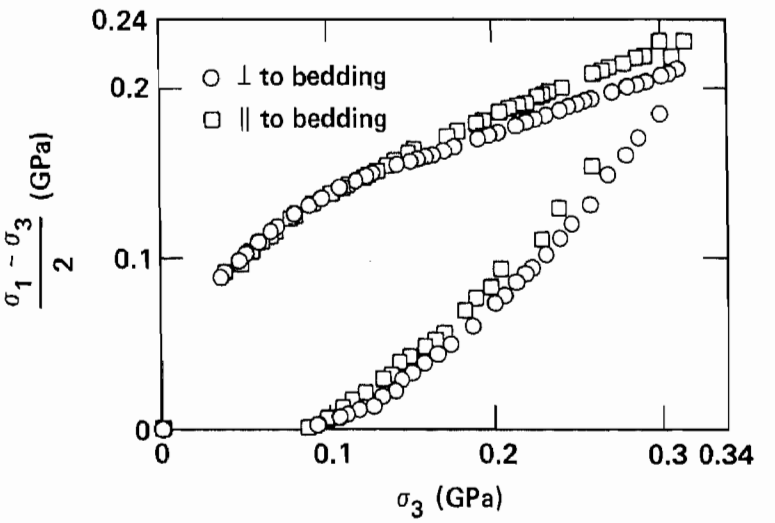

Fig. 16. Shear stress of Sandstone III under 1-D strain compression.

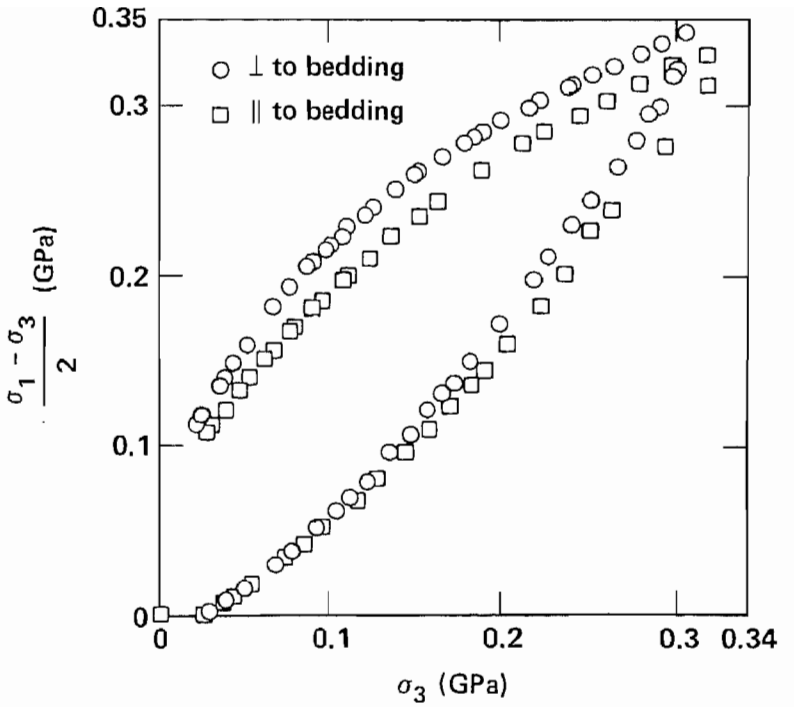

Fig. 17. Shear stress of Sandstone V under 1-D strain compression.